Data report: trace element, Sr isotope, and Ge/Si composition of fluids and sediments in ridge-flank low-temperature hydrothermal environments[1]

Samuel M. Hulme,[2] C. Geoffrey Wheat,[3,4] Rosalind M. Coggon,[5,6] and James McManus[7]

Chapter contents

[1]Hulme, S.M., Wheat, C.G., Coggon, R.M., and McManus, J., 2008. Data report: trace element, Sr isotope, and Ge/Si composition of fluids and sediments in ridge-flank low-temperature hydrothermal environments. *In* Fisher, A.T., Urabe, T., Klaus, A., and the Expedition 301 Scientists, *Proc. IODP,* 301: College Station, TX (Integrated Ocean Drilling Program Management International, Inc.). doi:10.2204/iodp.proc.301.202.2008
[2]Hawaii Institute of Geophysics and Planetology, 1680 East-West Road, POST 504, Honolulu HI 96822, USA. **hulme@hawaii.edu**
[3]Global Undersea Research Unit, PO Box 757220, University of Alaska Fairbanks, Fairbanks AK 99775, USA.
[4]Mailing address: PO Box 475, Moss Landing CA 95039, USA.
[5]School of Ocean and Earth Science, National Oceanography Centre, Southampton, University of Southampton, European Way, Southampton SO14 3ZH, United Kingdom.
[6]Present address: Department of Geological Sciences, University of Michigan, 2543 CC Little Building, 1100 North University, Ann Arbor MI 48109-1005, USA.
[7]College of Oceanic and Atmospheric Sciences, 104 Ocean Administration Building, Oregon State University, Corvallis OR 97331, USA.

Abstract

The data presented in this report demonstrate significant improvements in the ability to constrain trace element and Sr isotopic concentrations in sediments overlying ridge-flank hydrothermal systems. Improved sampling methods orchestrated by the Integrated Ocean Drilling Program (i.e., advanced piston coring and anoxic sample processing) enabled the collection of reactive pore water species with minimal alteration and sampling artifacts. Improved methods of high-resolution inductively coupled plasma–mass spectrometry trace element analysis, including the use of the 8-hydroxyquinoline functional group to extract and preconcentrate rare earth elements and other trace metals, were used to compile a data set of 28 trace element concentrations and $^{87}Sr/^{86}Sr$ ratios. From this extensive data set, we were able to increase the current understanding of how redox-reactive species respond to diagenic processes. Near-basement trends were used in combination with the known composition of hydrothermal fluids that exit Baby Bare Springs to asses our ability to predict basement fluid compositions using sediment pore water profiles collected by deep-sea drilling. The results show that prediction of basement fluid composition is possible for many trace elements, provided the near-basement concentration gradients are minimal. In order to place the Ge/Si systematics in a broader context, pore water and borehole fluid Ge and Si data are presented from additional sites across the Juan de Fuca Ridge flank and from two additional ridge-flank settings. These data show that Ge concentrations and Ge/Si ratios are much higher in the basement fluids than in the basal sediments because of increased mobilization of Ge relative to Si within the basement hydrothermal reservoir. Solid-phase sediment data are presented, highlighted by the occurrence of Mn- and carbonate-rich layers.

Introduction

Fluid circulation through oceanic crust plays a significant role in global geochemical, thermal, and tectonic processes (review in Fisher, 2005). Integrated Ocean Drilling Program (IODP) Expedition 301 was undertaken to constrain the hydrologic and geochemical processes within a ridge-flank hydrothermal setting by installing two new circulation obviation retrofit kits (CORKs) at IODP Site U1301, upgrading another CORK at Ocean Drilling Pro-

doi:10.2204/iodp.proc.301.202.2008

gram (ODP) Site 1026 (Fisher et al., 2005), and collecting sediment and basalt samples (see the **"Expedition 301 Summary"** chapter). IODP Site U1301 was selected based on previous investigations in the region (Hasselgren and Clowes, 1995; Davis, Fisher, Firth, et al., 1997; Elderfield et al., 1999) and the proximity to low-temperature hydrothermal springs to the north and south along a buried basement high (Mottl et al., 1998; Becker et al., 2000; Wheat et al., 2000, 2002). The approximate isothermal (~60°C) basement/sediment interface in this region of the Juan de Fuca Ridge (JFR) flank is attributed to vigorous fluid circulation through the uppermost ocean crust (Davis, Fisher, Firth, et al., 1997; Hutnak et al., 2006). In this report we present (1) trace element and Sr isotopic compositions of sediment pore fluids collected during Expedition 301; (2) concentrations of Ge in pore water and CORK fluid from reference sites on the eastern flanks of the JFR, southern East Pacific Rise (EPR), and Cocos Ridge; and (3) bulk sediment composition of the major and several minor elements, including Ge, from IODP Site U1301.

IODP Site U1301 pore fluids were extracted from whole-round sections obtained using the advanced piston corer (APC). Sediments were maintained in a nitrogen atmosphere during sample processing. After preliminary shipboard analysis of these fluids, it was apparent that the improved sampling techniques sufficiently preserved the concentrations of transition metal species (Mottl et al., 2000; Shipboard Scientific Party, 2004). On the basis of this observation, we undertook an extensive chemical analytical program that included many trace elements that were not measured on ODP Leg 168 pore fluids. These measurements were conducted in part to determine whether basal pore fluid concentrations and gradients for these trace elements can be used to predict the basement fluid composition, which is constrained by hydrothermal spring fluids from Baby Bare (Wheat et al., 2002) and borehole fluids from ODP Site 1026 (Wheat et al., 2004). The other topic of interest is the potential for biomediated geochemical exchange between the hydrothermal fluids, basement rocks, and overlying sediments affected by diagenetic processes (Bertine and Turekian, 1973; Morford and Emerson, 1999). Strontium isotope ratios ($^{87}Sr/^{86}Sr$) were measured to assess the extent of hydrothermal fluid–rock interactions because the Sr isotopic compositions of basalt and seawater are well known and distinct (~0.7025 and 0.70918, respectively).

Concentrations of Ge and Ge/Si molar ratios of pore and borehole fluids from other ridge-flank hydrothermal systems and bulk sediment chemical analyses from Site U1301 were conducted to elucidate Ge systematics within the crust. Pore water data from Site U1301 alone do not provide enough constraints for Ge in this setting. Ridge-flank hydrothermal systems could have an impact on Ge concentrations in the oceans and on using Ge as a proxy for paleoceanographic conditions (Wheat and McManus, 2005). These sites and samples include (1) pore and borehole fluid Ge concentrations from ODP Sites 1024 and 1025, which are located 25 and 35 km, respectively, from the JFR axis (Wheat et al., 2003, 2004); (2) borehole fluids from ODP Sites 1026 and 1027, which lie 100 and 105 km from the JFR axis and within kilometers of Site U1301 (Wheat et al., 2003, 2004); (3) pore waters extracted from sediment collected using a gravity core on the Cocos Ridge flank (Fisher et al., 2003; Parsons et al., submitted); and (4) pore waters extracted from sediment collected using a gravity core on the EPR flank (Grevemeyer et al., 2002). Pore waters from the latter two studies were extracted by centrifugation at 1°–4°C and filtered through a 0.45 µm filter. Lastly, bulk sediment chemical analyses were conducted on freeze-dried and ground sediments that were used for shipboard determinations of carbonate and organic carbon content.

Analytical methods

Dilution high-resolution inductively coupled plasma–mass spectrometry analysis

Rb, Mo, Cs, Ba, and U were analyzed in samples diluted to 1% in a solution of 10 mL/L that was made from diluting subboiled, concentrated (14.7 N) nitric acid (Optima grade) in 18.2 MΩ milli-Q (mQ) water (1% Q-HNO_3). Standard stock solution was made by combining aliquots of Claritas PPT standards in 1% Q-HNO_3. A Finnigan Element 2 high-resolution inductively coupled plasma–mass spectrometer (HR-ICP-MS), located at Moss Landing Marine Laboratories (MLML) (Moss Landing, California), was used for the analyses. The samples were introduced into the HR-ICP-MS through a CETAC Aridus desolvating nebulizer system fitted with a 100 µL/min nebulizer. Normalization of the data over varying plasma conditions was achieved by addition of internal standards (Rh and Tl).

Standard curves prepared in a 1% dilution of Pacific deep water exhibited negligible differences from those prepared in a salt-free solution. Recovery was within 95% with different matrix conditions and nearly 99% in Pacific deep water. Accuracy of these results was determined by analysis of two sets of previously analyzed samples: Mo and U measured in

Baby Bare hydrothermal spring water (Wheat et al., 2002) and Rb, Cs, and Ba measured in pore fluids from ODP Hole 1200F (Shipboard Scientific Party, 2002; Mottl et al., 2004). The average percent error between the two methods for each set of samples ranged between 0.7% for Rb and 8.2% for Mo. Precision was calculated as the standard deviation of Pacific deepwater subsamples that were analyzed periodically throughout a sample run. Detection limits, defined as three times the standard deviation of the blank, were calculated from procedural blanks.

Standard addition HR-ICP-MS analysis

Standard addition was performed on 10% dilutions of three 200 µL aliquots of samples diluted in 1% Q-HNO_3. This method was used to increase the detected counts per second for the transition metals V, Cr, Co, Ni, Cu, and Zn. Standard stock solution was created based on preliminary scans of the samples and diluted to 20% and 50% in 1% Q-HNO_3. A matrix-matched blank was produced by subjecting surface seawater to a column filled with 8-hydroxyquinoline (8-HQ), removing these metals from solution. Rhodium was added to all of the dilutions as an internal standard.

Analysis was conducted at MLML on a Finnigan Element 2 HR-ICP-MS with a 100 µL/min nebulizer fitted into a Teflon perfluoroalkoxyl copolymer resin spray chamber. A series of 10% dilutions of the metal-free seawater blanks were introduced into the HR-ICP-MS for 1 h prior to the start of the series to condition sample inlet cones on the HR-ICP-MS.

Accuracy of the standard addition analysis was determined by comparing the measured values of Pacific deep water (Wheat et al., 2002) for V and NASS-4 (National Research Council of Canada) standard reference material (SRM) for the remaining metals. The accuracy of Cr was the best (1.5% at 2.2 ng/kg), whereas the poorest was Ni (58% at 3.9 ng/kg). Precision was determined by calculating the standard deviation of results from repeated analyses of Pacific deep water. Detection limits were determined by multiplying the standard deviation of the metal-free seawater procedural blank by three.

Extraction HR-ICP-MS analysis

The extraction procedure for the rare earth elements (REEs), Y, and Cd revolved around the 8-HQ functional group immobilized onto TSK Fractogel (Fig. F1) (Landing et al., 1986; Measures et al., 1995; Dierssen et al., 2001). TSK Fractogel AF-Epoxy-600M was used to immobilize the 8-HQ ligand inside a column of Teflon wool within a 5 cm long section of 2 mm inner diameter silicon peristaltic pump tubing. The extraction apparatus, illustrated in Figure F1, sits inside a class-100 laminar flow clean bench to prevent contamination of the samples and reagents during extraction. The apparatus consists of two four-port and one eight-port, two-position injection valves (VICI Valco, Cheminert) controlled by microelectric actuators. Valve switches are controlled by a graphical user interface that dynamically adjusts the parameters controlling sample uptake volumes, column rinse times, and elution volumes. A peristaltic pump placed outside the clean bench pushes the samples and reagents through the apparatus at a constant rate, which is monitored gravimetrically.

Acidified samples were buffered to a pH of 5.3 (Sohrin et al., 1998) by in-line addition of an acetic acid and ammonium hydroxide solution (buffer solution: 84 mL ammonium hydroxide [Optima], 45 mL acetic acid [Optima], and 121 mL 18.2 MΩ mQ water) before the mixture was injected into the 8-HQ sample column. Once 4 mL of sample was introduced, the column was rinsed with 3 mL of 10% buffer solution diluted in mQ water to remove residual salts. After rinsing, the column was purged with air to minimize dilution of the eluate. A 0.5 mL volume of 1.12 N Q-HNO_3 eluant was used to extract elements off the 8-HQ column. Rh and Tl were added for internal standardization to the eluate, and the mass of samples and extracts were recorded. Between each sample extraction, the apparatus was reconditioned by rinsing the column and outflow tubing with 1.12 N Q-HNO_3 for a minimum of 10 min, while the remaining section of the apparatus was rinsed with 0.3 N Q-HNO_3. The column was then rinsed with the dilute buffer solution for 1 min prior to the next sample extraction to restore the pH of the column to 5.3.

Standards of Y, Cd, and REEs were added to filtered, acidified Pacific deep water in order to maintain a salt matrix within the standard solution during extraction. Standards were extracted in the same manner as the samples at the beginning and end of an analysis series, typically around 30–40 samples. Procedural blanks were produced every seventh sample by extracting 4 mL of mQ water into a vial containing an internal standard in the same method used for samples and standards. Analysis of the eluates by HR-ICP-MS was conducted on the Element 2 HR-ICP-MS at MLML through the Aridus desolvating nebulizer with a 100 µL/min nebulizer.

Column recovery within the first 0.5 mL of eluate was generally >97%, ranging between complete recovery of Ho and only 95% recovery of Ce. Accuracy of the method was determined by analyzing a Pacific deepwater sample that had been previously analyzed at Oregon State University (Wheat et al., 2002) and

was within the margin of error of the differing analyses. Precision was determined by the standard deviation of Pacific deep water analyzed every seventh sample. Detection limits are calculated by multiplying the standard deviation of daily procedural blanks by three. Additional details of the method are included in Hulme (2005).

Sr isotopic analysis

Strontium isotopic compositions were determined by thermal ionization mass spectrometry (TIMS) at the National Oceanography Centre, Southampton. Strontium was separated from pore fluid samples by standard ion-exchange procedures. Aliquots of pore fluid were evaporated to incipient dryness and redissolved in 0.2 mL of 3 M HNO_3. Strontium was isolated with 80 µL Sr-Spec columns and eluted with 3 M HNO_3. Sr samples were loaded onto outgassed Ta filaments using a Ta activator solution and analyzed in multidynamic mode using a VG sector 54 TIMS. The average value of $^{87}Sr/^{86}Sr$ for National Institute of Standards SRM (NIST)-987 on this instrument was 0.710255 ± 0.000026 (2σ) for the period of the analyses (N = 54), and Sr-Spec column blanks were <0.07 ng.

Pore water Ge analysis

Inorganic Ge (germanic acid) was measured using an isotope dilution technique (Mortlock and Froelich, 1996; Hammond et al., 2000) at Oregon State University (OSU) W.M. Keck Collaboratory on a VG ExCell quadrupole ICP-MS. Samples were diluted (0.1–1 mL) and spiked with ^{70}Ge to a final sample volume of 20 mL. After sample equilibration, germanic acid is then converted to germane (GeH_4) in a reaction chamber using sodium borohydride, which is transferred using a He carrier to a glass trap submerged in liquid nitrogen. Upon subsequent warming the germane is injected into an ICP-MS. The 7% relative error posted is the average error from running duplicates of samples at varying concentrations; however, because it is difficult to predict, a priori, the Ge concentration of these samples, we use a range of sample/spike volumes. As a result, our variability was >7% (up to 15%) for samples with high concentrations of Ge when the range of sample/spike fluid ratios that were used were not in reasonable proportion to the sample Ge concentration (Mortlock et al., 1993).

Bulk sediment analysis

Analysis of sediment elemental compositions was conducted at OSU. Because Si can be lost via volatilization during HF digestions, sediment samples were digested using a "fusion" technique (Murray et al., 2000). This technique uses ~800 mg of Li metaborate and ~200 mg of sample. Samples are then fused at 1100°C for 15–20 min and then dissolved in 2 N HNO_3. This technique was compared to two other hot acid digestion techniques to ascertain compatibility with other methods (McManus et al., 2006). Results of the comparison were found to be analytically indistinguishable among the three techniques, and reasonable agreement was obtained for SRMs (McManus et al., 2006).

Results

Results are presented in Tables **T1, T2, T3, T4,** and **T5** and Figures **F2, F3,** and **F4.** At IODP Site U1301, all of the trace elements that were analyzed in the pore fluids, with the exception of U, were mobilized within the sediment column to concentrations above those in bottom seawater (shown as 0 depth in Fig. **F2**). Transition metals and REEs exhibited maximum values in the upper to middle sediment column as a result of redox conditions produced during diagenesis (Haley et al., 2004). Cr, Cs, and Cd concentrations peaked sharply in the lower zone of sulfate reduction at 170.1 m (Cr = 10.4 nmol/kg, Cs = 14.6 nmol/kg, and Cd = 7700 pmol/kg). A majority of the trace element gradients in basal sediments approach calculated concentrations at the sediment/basaltic interface that are close to concentrations in Baby Bare Spring fluids, which represent pristine formation fluid compositions (Wheat et al., 2002). Concentrations of Rb and Cs in basal sediments are clearly lower than predicted basement concentrations (Rb: 222 vs. 1120 nmol/kg; Cs: 0.95 vs. 5.3 nmol/kg), which could be attributed to continued alteration of the basement fluids associated with the exchange of the major constituents K and Na with Ca (Elderfield et al., 1999). Basal pore fluid concentrations of Ni (133 nmol/kg), Zn (290 nmol/kg), Mo (435 nmol/kg), Ba (800 nmol/kg), and La (119 pmol/kg) are significantly above those predicted by Baby Bare Spring compositions. This could be a result of steep concentration gradients near the basement, resulting in a larger uncertainty, as observed in the Mn data (Shipboard Scientific Party, 2004). In cases where there is no discernable gradient near the basement (e.g., Mo; Fig. **F2**), the overestimation of predicted values can be attributed to increases in basement fluid concentrations along this transect, similar to those recorded for the major and minor species (Wheat et al., 2000).

The Sr isotopic compositions of IODP Site U1301 pore waters range from near seawater values in the uppermost sediments (0.709138) to more evolved compositions with a clear basaltic $^{87}Sr/^{86}Sr$ signature

deeper in the sedimentary section. The $^{87}Sr/^{86}Sr$ profile is similar in shape to that of nearby ODP Hole 1027B (Mottl et al., 2000) in crust of similar age and upper basement temperature (~3.6 Ma and 63°C) (Davis, Fisher, Firth, et al., 1997), with a local $^{87}Sr/^{86}Sr$ ratio maximum (0.708163) at 78.7 meters below seafloor (mbsf) and a local minimum (0.707609) between 190 and 240 mbsf. The lowermost pore water sample has an $^{87}Sr/^{86}Sr$ ratio of 0.707609, similar to that of Baby Bare Spring fluids (~0.70745) (Butterfield et al., 2001) and ODP Hole 1026B basement fluid (~0.70739) (Elderfield et al., 1999). The similar Sr isotopic composition of in situ basement fluid at ODP Site 1026 and basement fluids venting at Baby Bare to the IODP Site U1301 near-basement pore fluid is consistent with near-basement pore fluids being representative of upper basement ridge-flank hydrothermal fluids. This result is consistent with conclusions derived from Sr isotopic and trace element compositions of basement-hosted calcium carbonate veins and near-basement pore fluids from ODP Sites 1025–1028 and 1032 (Coggon et al., 2004).

Concentrations of inorganic Ge dissolved in pore fluids often mirror Ge/Si molar ratios (Figs. **F2, F3**). Maximum values of both in the pore fluids occur in IODP Hole U1301C, with 4800 pmol/kg Ge and 12.3 Ge/Si (µmol/mol). In IODP Hole U1301C, both values increased in the basal sediments, whereas the opposite trend existed at ODP Sites 1024 and 1025. Despite this apparent contradiction, borehole fluids at all three sites contained Ge/Si ratios many factors above any ratio in the pore fluids. Of particular interest is the relatively low concentrations of Ge in the ODP Site 1024 CORK fluids, yet Ge/Si molar ratios are nearly four times greater than any of the pore fluid ratios. The highest values for dissolved Ge concentrations and Ge/Si molar ratios both occur in the basement fluids recovered from CORKs (22,300 pmol/kg at ODP Site 1026 and 68 µmol/mol at ODP Site 1027). Pore fluid Ge concentrations and Ge/Si molar ratios in gravity cores from the southern EPR flank were minimally altered from bottom seawater with the lowest values measured from any of the locations (46 pmol/kg and 0.26 µmol/mol). Pore waters from the flanks of the Cocos Ridge display Ge and Ge/Si patterns similar to those observed in surficial sediments at ODP Sites 1024 and 1025.

Solid-phase sediment compositions are presented in Table **T5** and Figure **F4.** The most striking characteristic of the sediment chemistry is a carbonate- and Mn-rich layer at 184.1 mbsf, corresponding to minima in Si (82,100 mg/kg), Mg (8,100 mg/kg), Fe (19,600 mg/kg), Al (28,700 mg/kg), Ti (1,530 mg/kg), and Ge (0.215 mg/kg). Mn shows a clear local maximum at 184.1 mbsf, but the greatest enrichment (5830 mg/kg) occurs in the basal sediments at 243.3 mbsf. Ge/Si ratios do not appear to be as closely correlated with variations in Si content.

Acknowledgments

The authors would like to thank Moss Landing Marine Laboratories and Mike Gordon for the use of their HR-ICP-MS facilities and advice on optimizing the trace element analyses. This research used samples and/or data provided by the Integrated Ocean Drilling Program (IODP). Funding was provided by IODP, a grant from the Joint Oceanographic Institutions U.S. Science Support Program, and by Natural Environmental Research Council grant NE/C513242/1 to Damon A.H. Teagle and R.M. Coggon. This is Hawaii Institute of Geophysics and Planetology contribution 1496 and SOEST contribution 7164.

References

Becker, N.C., Wheat, C.G., Mottl, M.J., Karsten, J.L., and Davis, E.E., 2000. A geological and geophysical investigation of Baby Bare, locus of a ridge flank hydrothermal system in the Cascadia Basin. *J. Geophys. Res.,* 105(B10):23557–23568. **doi:10.1029/2000JB900204**

Bertine, K.K., and Turekian, K.K., 1973. Molybdenum in marine deposits. *Geochim. Cosmochim. Acta,* 37(6):1415–1434. **doi:10.1016/0016-7037(73)90080-X**

Butterfield, D.A., Nelson, B.K., Wheat, C.G., Mottl, M.J., and Roe, K.K., 2001. Evidence for basaltic Sr in mid-ocean ridge-flank hydrothermal systems and implications for the global oceanic Sr isotope balance. *Geochim. Cosmochim. Acta.,* 65(22):4141–4153. **doi:10.1016/S0016-7037(01)00712-8**

Coggon, R.M., Teagle, D.A.H., Cooper, M.J., and Vanko, D.A., 2004. Linking basement carbonate vein compositions to porewater geochemistry across the eastern flank of the Juan de Fuca Ridge, ODP Leg 168. *Earth Planet. Sci. Lett.,* 219(1–2):111–128. **doi:10.1016/S0012-821X(03)00697-6**

Davis, E.E., Fisher, A.T., Firth, J.V., et al., 1997. *Proc. ODP, Init. Repts.,* 168: College Station, TX (Ocean Drilling Program). **doi:10.2973/odp.proc.ir.168.1997**

Dierssen, H., Balzer, W., and Landing, W.M., 2001. Simplified synthesis of an 8-hydroxyquinoline chelating resin and a study of trace metal profiles from Jellyfish Lake, Palau. *Mar. Chem.,* 73(3–4):173–192. **doi:10.1016/S0304-4203(00)00107-9**

Elderfield, H., Wheat, C.G., Mottl, M.J., Monnin, C., and Spiro, B., 1999. Fluid and geochemical transport through oceanic crust: a transect across the eastern flank of the Juan de Fuca Ridge. *Earth Planet. Sci. Lett.,* 172(1–2):151–165. **doi:10.1016/S0012-821X(99)00191-0**

Fisher, A.T., 2005. Marine hydrogeology: recent accomplishments and future opportunities. *Hydro. J.,* 13(1):69–97. **doi:10.1007/s10040-004-0400-y**

Fisher, A.T., Stein, C.A., Harris, R.N., Wang, K., Silver, E.A., Pfender, M., Hutnak, M., Cherkaoui, A., Bodzin, R., and Villinger, H., 2003. Abrupt thermal transition reveals hydrothermal boundary and role of seamounts within the Cocos plate. *Geophys. Res. Lett.,* 30(11):1550–1553. **doi:10.1029/2002GL016766**

Fisher, A.T., Urabe, T., Klaus, A., and the IODP Expedition 301 Scientists, 2005. IODP Expedition 301 installs three borehole crustal observatories, prepares for three-dimensional, cross-hole experiments in the northeastern Pacific Ocean. *Sci. Drill.,* 1:6–11. **doi:10.2204/iodp.sd.1.01.2005**

Grevemeyer, I., Schramm, B., Devey, C.W., Wilson, D.S., Jochum, B., Hauschild, J., Aric, K., Villinger, H.W., and Weigel, W., 2002. A multibeam-sonar, magnetic and geochemical flowline survey at 14°14′S on the southern East Pacific Rise: insights into the fourth dimension of ridge crest segmentation. *Earth Planet. Sci. Lett.,* 199(3–4):359–372. **doi:10.1016/S0012-821X(02)00595-2**

Haley, B., Klimkhammer, G.P., and McManus, J., 2004. Rare earth elements in pore waters of marine sediments. *Geochim. Cosmochim. Acta,* 68(6):1265–1279. **doi:10.1016/j.gca.2003.09.012**

Hammond, D.E., McManus, J., Berelson, W.M., Meredith, C., Klinkhammer, G.P., and Coale, K.H., 2000. Diagenetic fractionation of Ge and Si in reducing sediments: the missing Ge sink and a possible mechanism to cause glacial/interglacial variations in oceanic Ge/Si. *Geochim. Cosmochim. Acta.,* 64(14):2453–2465. **doi:10.1016/S0016-7037(00)00362-8**

Hasselgren, E.O., and Clowes, R.M., 1995. Crustal structure of northern Juan de Fuca plate from multichannel reflection data. *J. Geophys. Res.,* 100(B4):6469–6486. **doi:10.1029/94JB02941**

Hulme, S.M., 2005. Sources and magnitude of fluid venting from the Mariana forearc serpentine mud volcanoes [M.S. thesis]. San Jose State Univ., California.

Hutnak, M., Fisher, A.T., Zühlsdorff, L., Spiess, V., Stauffer, P.H., and Gable, C.W., 2006. Hydrothermal recharge and discharge guided by basement outcrops on 0.7–3.6 Ma seafloor east of the Juan de Fuca Ridge: observations and numerical models. *Geochem., Geophys., Geosyst.,* 7(7):Q07O02. **doi:10.1029/2006GC001242**

Landing, W.M., Haraldsson, C., and Paxeus, N., 1986. Vinyl polymer agglomerate based transition metal cation-chelating ion-exchange resin containing the 8-hydroxyquinoline functional group. *Anal. Chem.,* 58(14):3031–3035. **doi:10.1021/ac00127a029**

McManus, J., Berelson, W.M., Severmann, S., Poulson, R.L., Hammond, D.E., Klinkhammer, G.P., and Holm, C., 2006. Molybdenum and uranium geochemistry in continental margin sediments: paleoproxy potential. *Geochim. Cosmochim. Acta.,* 70(18):4643–4662. **doi:10.1016/j.gca.2006.06.1564**

Measures, C.J., Yuan, J., and Resing, J.A., 1995. Determination of iron in seawater by flow injection analysis using in-line preconcentration and spectrophotometric detection. *Mar. Chem.,* 50(1–4):3–12. **doi:10.1016/0304-4203(95)00022-J**

Morford, J.L., and Emerson, S, 1999. The geochemistry of redox sensitive trace metals in sediments. *Geochim. Cosmochim. Acta,* 63(11–12):1735–1750. **doi:10.1016/S0016-7037(99)00126-X**

Mortlock, R.A., and Froelich, P.N., 1996. Determination of germanium by isotope dilution-hydride generation inductively coupled plasma mass spectrometry. *Anal. Chim. Acta,* 332(2–3):277–284. **doi:10.1016/0003-2670(96)00230-9**

Mortlock R.A., Froelich, P.N., Feely, R.A., Massoth, G.J., Butterfield, D.A., and Lupton, J.E., 1993. Silica and germanium in Pacific Ocean hydrothermal vents and plumes. *Earth Planet. Sci. Lett.,* 119(3):365–378. **doi:10.1016/0012-821X(93)90144-X**

Mottl, M.J., Wheat, C.G., Baker, E., Becker, N., Davis, E., Feely, R., Grehan, A., Kadko, D., Lilley, M., Massoth, G., Moyer, C., and Sansone, F., 1998. Warm springs discovered on 3.5 Ma oceanic crust, eastern flank of the Juan de Fuca Ridge. *Geology,* 26(1):51–54. **doi:10.1130/0091-7613(1998)026<0051:WSDOMO>2.3.CO;2**

Mottl, M.J., Wheat, C.G., Fryer, P., Gharib, J., and Martin, J.B., 2004. Chemistry of springs across the Mariana forearc shows progressive devolatilization of the subducting plate. *Geochim. Cosmochim. Acta,* 68(23):4915–4933. **doi:10.1016/j.gca.2004.05.037**

Mottl, M.J., Wheat, C.G., Monnin, C., and Elderfield, H., 2000. Data report: trace elements and isotopes in pore water from Sites 1023 through 1032, eastern flank of the Juan de Fuca Ridge. *In* Fisher, A., Davis, E.E., and Escutia, C. (Eds.), *Proc. ODP, Sci. Results,* 168: College Station, TX (Ocean Drilling Program), 105–115. **doi:10.2973/odp.proc.sr.168.019.2000**

Murray, R.W., Miller, D.J., and Kryc, K.A., 2000. Analysis of major and trace elements in rocks, sediments, and interstitial waters by inductively coupled plasma–atomic emission spectrometry (ICP-AES). *ODP Tech. Note,* 29. **doi:10.2973/odp.tn.29.2000**

Parsons, P.K.F., Wheat, C.G., Fisher, A.T., Silver, E.A., Underwood, M., and Hutnak, M., submitted. Hydrothermal seepage of altered crustal fluids seaward of the Middle America Trench, offshore Costa Rica. *J. Geophs. Res.*

Shipboard Scientific Party, 2002. Site 1200. *In* Salisbury, M.H., Shinohara, M., Richter, C., et al., *Proc. ODP, Init. Repts.,* 195: College Station, TX (Ocean Drilling Program), 1–173. **doi:10.2973/odp.proc.ir.195.103.2002**

Shipboard Scientific Party, 2004. Juan de Fuca hydrogeology: the hydrogeologic architecture of basaltic oceanic crust: compartmentalization, anisotropy, microbiology, and crustal-scale properties on the eastern flank of Juan de Fuca Ridge, eastern Pacific Ocean. *IODP Prel. Rept.,* 301. **doi:10.2204/iodp.pr.301.2004**

Sohrin, Y., Iwamoto, S.-I., Akiyama, S., Fujita, T., Kugii, T., Obata, H., Nakayama, E., Goda, S., Fujishima, Y., Hasegawa, H., Ueda, K., and Matsui, M., 1998. Determination of trace elements in seawater by fluorinated metal alkoxide glass-immobilized 8-hydroxyquinoline concentration and high-resolution inductively coupled plasma mass spectrometry detection. *Anal. Chim. Acta,* 363(1):11–19. **doi:10.1016/S0003-2670(98)00074-9**

Wheat, C.G., Elderfield, H., Mottl, M.J., and Monnin, C., 2000. Chemical composition of basement fluids within an oceanic ridge flank: implications for along-strike and across-strike hydrothermal circulation. *J. Geophys. Res.,* 105(B6):13437–13448. **doi:10.1029/2000JB900070**

Wheat, C.G., Jannasch, H.W., Kastner, M., Plant, J.N., and DeCarlo, E.H., 2003. Seawater transport and reaction in upper oceanic basaltic basement: chemical data from continuous monitoring of sealed boreholes in a ridge flank environment. *Earth Planet. Sci. Lett.,* 216(4):549–564. **doi:10.1016/S0012-821X(03)00549-1**

Wheat, C.G., Jannasch, H.W., Kastner, M., Plant, J.N., DeCarlo, E.H., and Lebon, G., 2004. Venting formation fluids from deep-sea boreholes in a ridge flank setting: ODP Sites 1025 and 1026. *Geochem., Geophys., Geosyst.,* 5(8):Q08007. **doi:10.1029/2004GC000710**

Wheat, C.G., and McManus, J., 2005. The potential role of ridge-flank hydrothermal systems on oceanic germanium and silicon balances. *Geochim. Cosmochim. Acta,* 69(8):2021–2029. **doi:10.1016/j.gca.2004.05.046**

Wheat, C.G., Mottl, M.J., and Rudnicki, M., 2002. Trace element and REE composition of a low-temperature ridge-flank hydrothermal spring. *Geochim. Cosmochim. Acta,* 66(21):3693–3705. **doi:10.1016/S0016-7037(02)00894-3**

Initial receipt: 7 April 2007
Acceptance: 17 October 2007
Publication: 15 February 2008
MS 301-202

Figure F1. Schematic diagram of the apparatus used for extraction of trace elements from fluid samples by immobilization onto 8-hydroxyquinoline columns (shown as 8-HQ). The pumping direction is from left to right and the calibrated flow rates are shown for each peristaltic pump tubing line. Switching of the valves was controlled by a graphic user interface software program to cycle the system through the entire extraction process after placing the sample in the uptake slot. Solution compositions are provided in the text. mQ = 18.2 MΩ water.

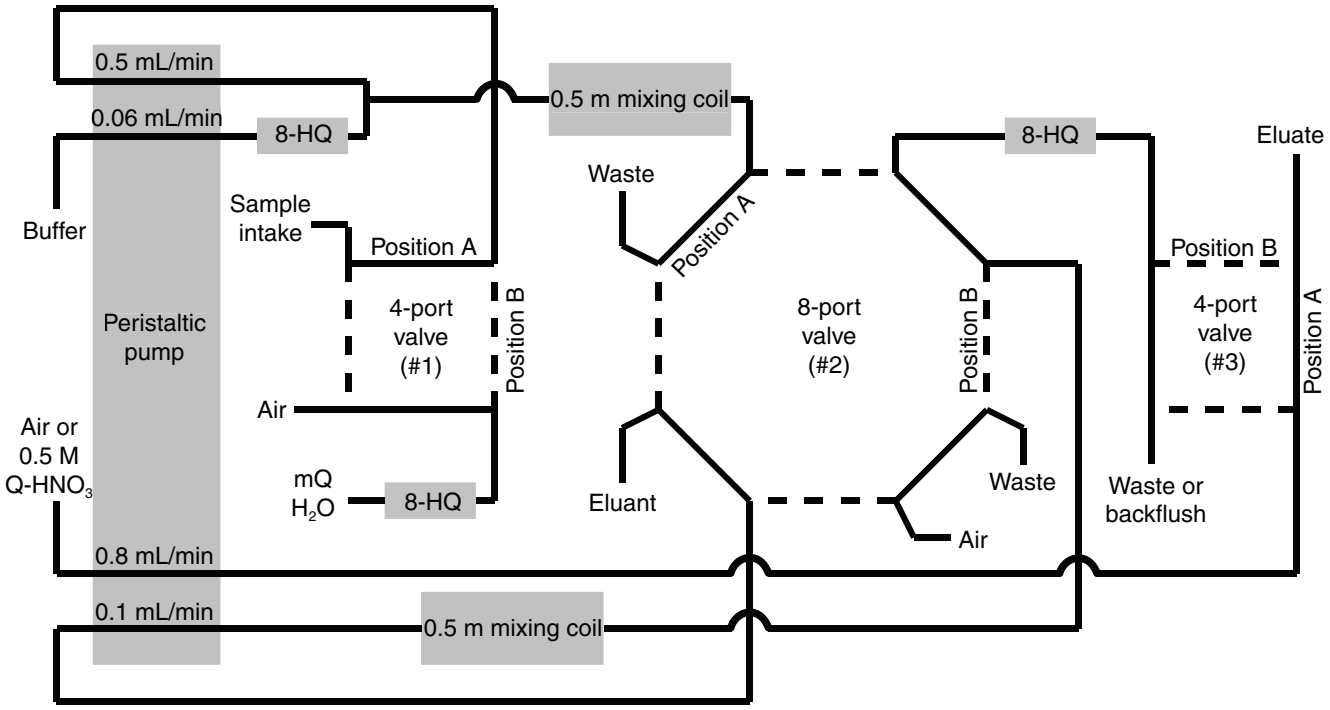

Figure F2. Trace element profiles of pore fluids extracted from IODP Site U1301. Solid symbols = Baby Bare Spring fluid compositions from Wheat et al. (2002). Error bars (1σ) are included for each datum; however, in many cases the symbols are greater than one standard deviation of the analyses. (Continued on next page.)

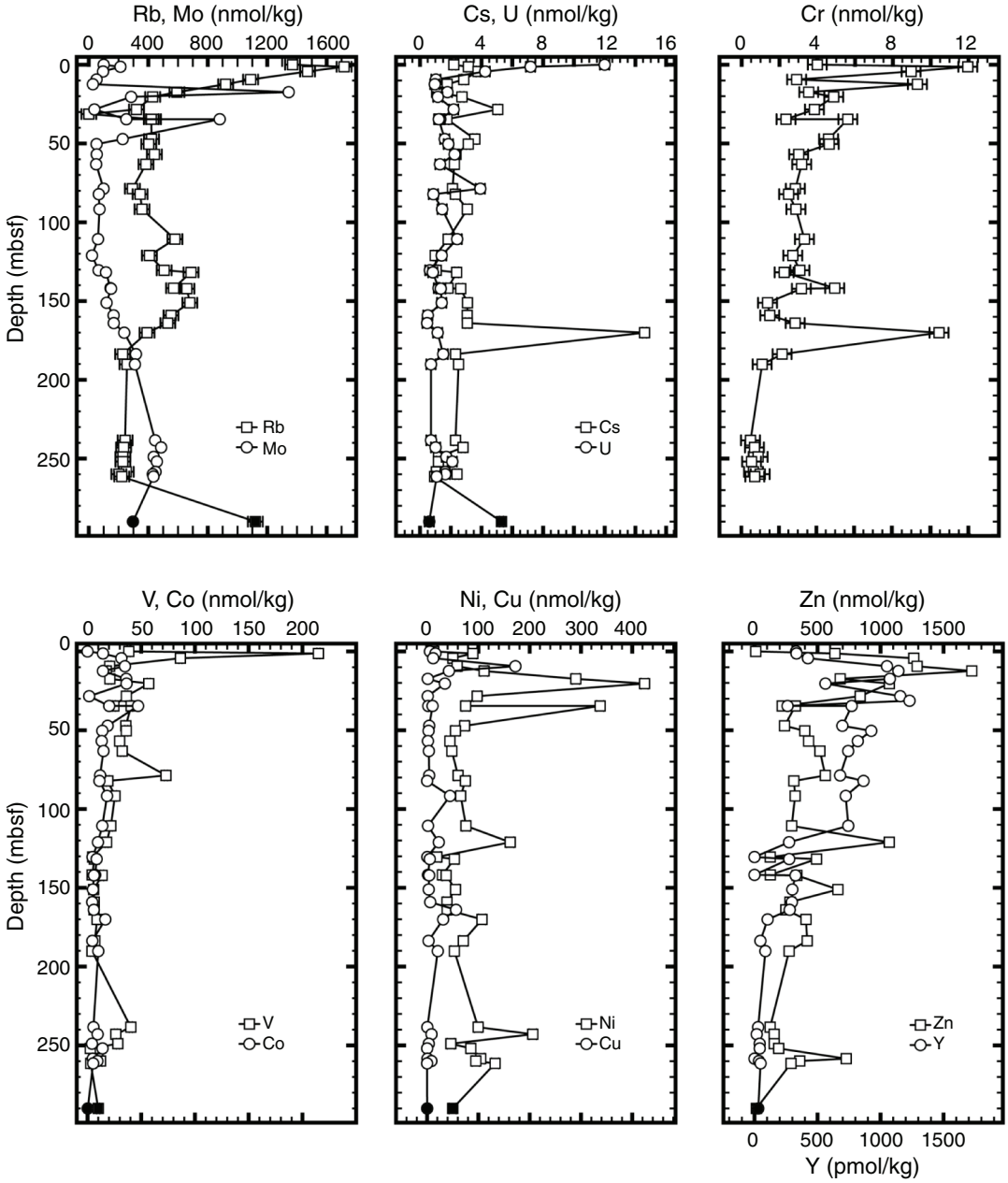

Figure F2 (continued).

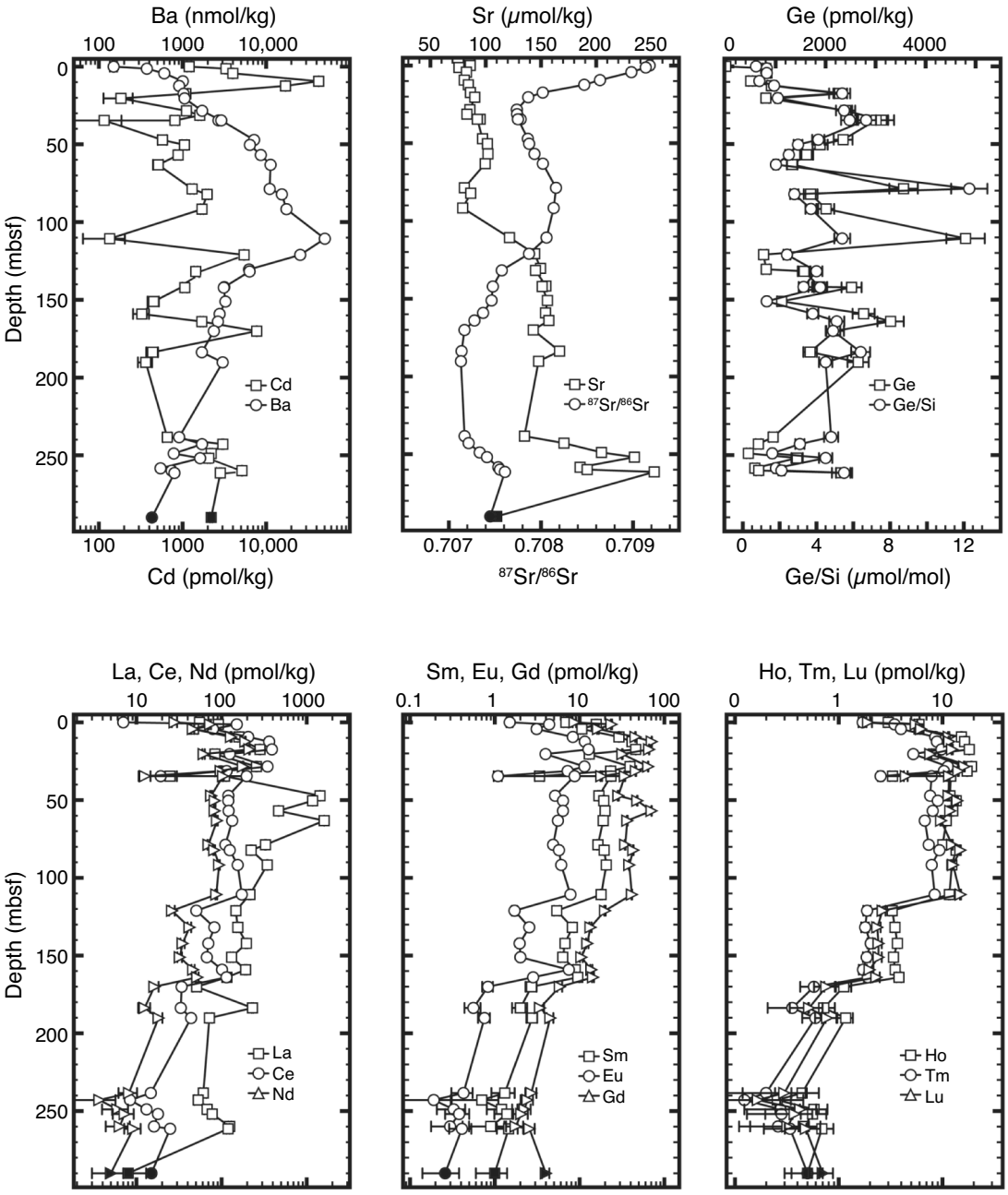

Figure F3. Depth profiles of Ge concentrations and Ge/Si molar ratios in pore fluids from ridge-flank sediments. ODP Sites 1024 and 1025 samples are from the Juan de Fuca Ridge (Davis, Fisher, Firth, et al., 1997). TicoFlux samples are from the Cocos Ridge flank (Fisher et al., 2003). EXCO samples are from the eastern flank of the East Pacific Rise (Grevemeyer et al., 2002). Error bars (1σ) are included but are often smaller than the size of the symbol.

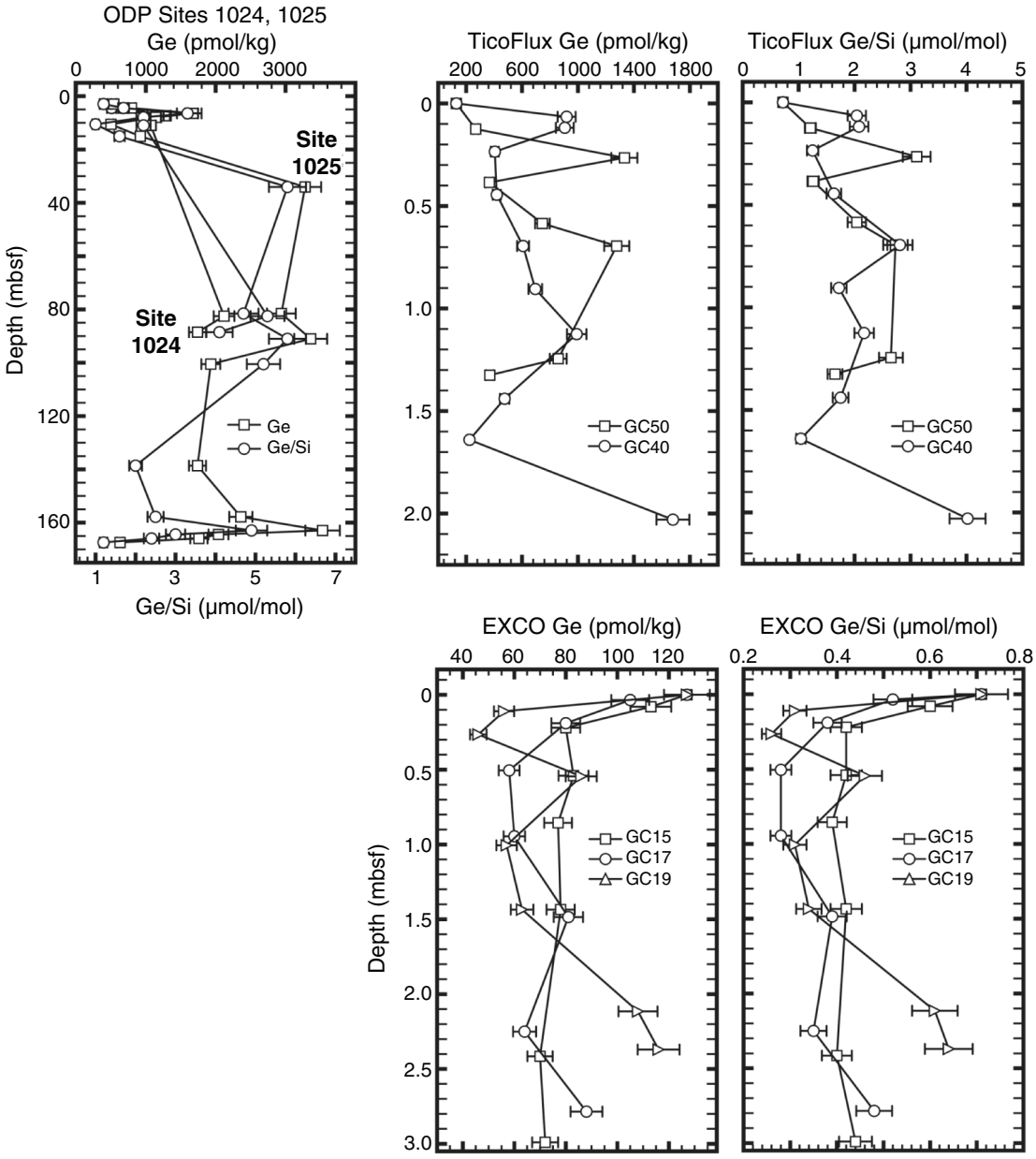

Figure F4. Bulk sediment chemistry from IODP Hole U1301C analyzed by inductively coupled plasma–atomic emission spectroscopy and ICP-MS. Relative error bars (1σ) are included but often obscured by the symbols.

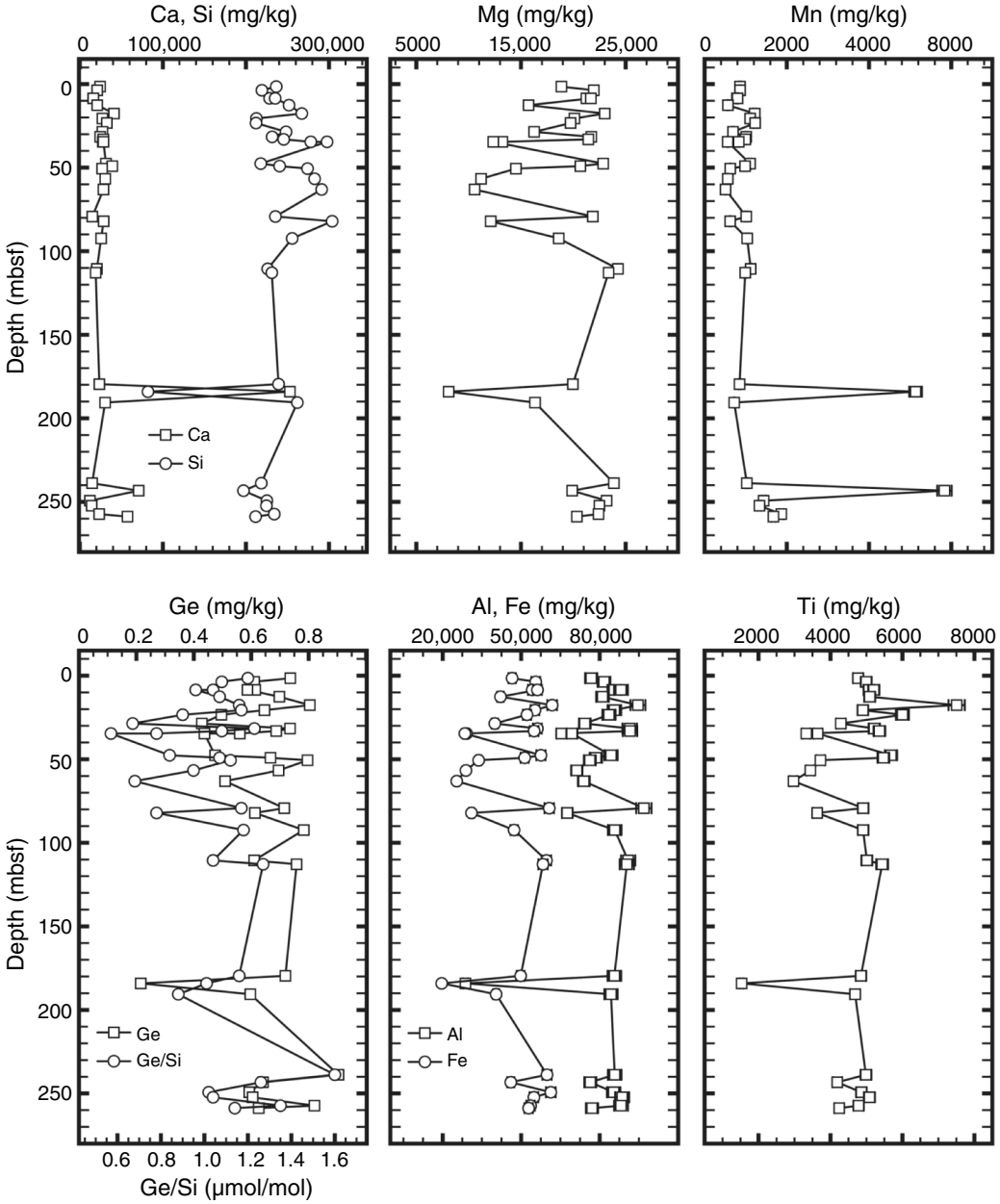

Table T1. Trace element and Sr isotope composition of pore water, Site U1301. (Continued on next page.)

Core, section, interval (cm)	Depth (mbsf)	HR-ICP-MS 1% dilutions (nmol/kg)					HR-ICP-MS standard addition (nmol/kg)						$^{87}Sr/^{86}Sr$	Ge (pmol/kg)	Ge/Si (µmol/mol)
		Rb	Mo	Cs	Ba	U	V	Cr	Co	Ni	Cu	Zn			
301-U1301C-															
1H-1, 130–150	1.3	1720	213	3.15	374	7.2	215.0	12.0	14.4	89	16.3	638	0.709138	803	1.29
1H-3, 130–150	4.3	1470	96	3.78	604	4.2	86.5	9.0	31.5	50	11.8	1260	0.708982	828	1.34
2H-3, 130–150	9.4	1090	52	2.84	1,010	1.0	20.6	2.9	34.8	59	172	1290	0.708641	501	0.89
2H-5, 130–150	12.4	920	27	1.77	910	1.0	17.6	9.3	14.4	111	42.7	1720	0.708470	916	1.74
3H-2, 130–150	17.4	593	1340	1.08	1,030	1.8	20.8	3.5	36.0	290	1.4	680	0.708019	2250	5.42
3H-4, 130–150	20.4	429	285	2.73	1060	1.2	57.0	4.9	36.3	424	34.7	1070	0.707861	804	1.91
4H-3, 130–150	28.4	320	38	5.05	1,700	2.2	36.2	3.8	1.57	98	1.3	838	0.707738	2400	5.50
4H-5, 130–150	31.3	NA	NA	NA	NA	NA	NA	NA	NA	NA	NA	NA	0.707741	NA	NA
5H-2 mud, 0–40	34.6	435	252	1.72	2,690	1.3	24.5	2.3	20.2	75	2.3	220	0.707779	3120	5.84
5H-2 sand, 0–40	34.6	420	880	1.75	2,900	1.2	40.6	5.6	47.1	337	10.7	324	0.707750	3010	6.69
6H-3, 110–150	47.7	422	228	3.56	7,160	1.6	35.7	4.6	18.7	73	4.2	238	0.707857	2350	4.15
6H-5, 110–150	50.4	403	52	3.14	6,381	1.8	36.1	4.6	13.8	55	2.9	398	0.707871	1890	2.98
7H-3, 110–150	56.9	441	53	2.34	8,620	2.2	29.9	3.0	13.2	44	1.7	429	0.707929	1620	2.45
8H-1, 110–150	63.2	384	49	2.23	11,300	1.3	32.3	3.2	14.9	48	3.5	519	0.708020	1330	1.76
9H-5, 110–150	78.7	293	99	2.11	11,000	3.9	73.0	2.8	11.7	60	4.1	562	0.708163	3560	12.3
10H-1, 110–150	82.2	345	67	2.30	15,400	0.9	18.9	2.5	11.1	75	0.1	313	NA	1700	2.79
11H-1, 110–150	91.7	358	72	3.08	17,500	1.4	25.6	2.9	18.2	66	44.8	323	0.708138	2010	3.74
13H-1, 110–150	110.7	579	62	1.83	50,200	2.4	21.7	3.3	13.8	76	1.8	295	0.708060	4800	5.41
15H-1, 110–150	179.2	270	383	3.33	2,270	2.7	10.9	0.6	3.26	45	0.3	109	0.707170	1690	6.35
15H-4, 110–150	183.7	228	317	2.31	1,700	1.5	6.8	2.1	4.51	71	2.9	418	0.707138	NA	NA
16H-2, 110–150	190.2	257	310	2.51	3,020	0.7	4.2	1.1	10.0	53	20.9	274	0.707131	2650	4.52
17H-2, 110–150	238.4	244	446	2.31	910	0.7	40.3	0.5	5.55	100	0.5	124	0.707171	950	4.84
17H-5, 110–150	242.9	234	486	2.80	1,710	1.0	26.4	0.7	9.43	206	8.7	156	0.707215	655	3.13
18H-2, 110–150	248.9	229	436	1.20	784	1.7	28.2	0.9	4.17	46	3.3	156	0.707335	454	1.60
18H-4, 110–150	251.9	229	458	1.19	1,620	2.1	2.6	0.5	14.0	85	0.2	192	0.707414	1430	4.45
19H-1, 110–150	256.9	364	266	1.07	532	7.4	10.3	0.4	3.40	37	0.6	354	0.707828	422	1.83
19H-2, 110–150	258.4	252	449	1.06	545	1.6	9.7	0.6	4.90	105	0.8	728	0.707537	584	1.81
19H-3, 110–150	259.9	202	430	2.40	741	1.6	12.1	1.0	9.21	95	8.4	359	0.707555	661	2.14
19H-4, 110–150	261.4	222	435	0.95	800	1.1	3.0	0.7	5.27	133	0.1	290	0.707609	2310	5.50
301-U1301D-															
1H-1, 110–150	121.1	407	21	0.99	25,500	1.4	17.7	2.7	9.71	162	22.9	1070	0.707870	759	2.38
2H-1, 98–118	130.5	507	66	1.05	6,240	0.6	4.8	3.1	4.68	19	0.5	125	NA	811	NA
2H-2, 110–150	131.8	687	115	2.38	6,320	0.8	6.4	2.2	8.49	53	5.2	492	0.707575	1570	4.00
3H-2, 132–150	141.8	571	146	1.82	3,150	1.2	4.3	4.9	7.11	30	1.8	126	NA	1880	3.27
3H-3, 14–54	142.1	659	150	2.65	3,110	1.3	13.6	3.2	5.94	37	4.1	336	0.707478	2520	4.17
4H-2, 110–150	151.1	680	119	3.09	3,260	1.4	5.6	1.4	5.06	55	3.2	662	0.707464	1120	1.32
5H-1, 110–150	159.1	553	167	3.07	2,770	0.5	6.2	1.5	4.40	39	6.2	281	0.707374	2760	3.76
5H-5, 0–40	164.0	531	168	3.07	2,650	0.5	6.1	2.8	5.87	39	56.4	249	0.707372	3300	5.05
6H-2, 110–150	170.1	392	238	14.6	2,360	1.1	8.9	10.4	16.6	107	31.3	408	0.707278	2190	4.94
Error (±)		50	6	0.13	15	0.3	1.4	0.5	0.012	7	1.8	3	0.000016	7%	8%
Detection limit		5	1.3	0.12	10	0.01	0.16	0.3	0.05	9	1.5	2			
Bottom seawater		1296	119	1.85	140	12.3	36.7	4.9	0.07	20	8.1	17	0.7084	115	0.72

Notes: Errors given for elemental concentrations are 1σ of the bottom seawater concentrations shown. Sr isotopic error is the maximum of the individual standard errors for the sample set. HR-ICP-MS = high-resolution inductively coupled plasma–mass spectrometer. NA = not analyzed.

Table T1 (continued).

Core, section, interval (cm)	Depth (mbsf)	HR-ICP-MS 8-HQ extractions (pmol/kg)															
		Y	Cd	La	Ce	Pr	Nd	Sm	Eu	Gd	Tb	Dy	Ho	Er	Tm	Yb	Lu
301-U1301C-																	
1H-1, 130–150	1.3	333	3,300	92	151	16.5	73	15.7	4.37	23.7	3.04	34.6	5.9	21.7	3.45	27.3	5.52
1H-3, 130–150	4.3	424	3,990	47	79.1	9.8	46	10.7	3.11	16.5	2.47	30.1	5.9	23.6	3.97	33.3	6.19
2H-3, 130–150	9.4	1050	42,400	159	205	28.1	129	29.1	8.32	45.6	7.08	86.7	15.2	55.4	8.52	66.0	11.5
2H-5, 130–150	12.4	1140	17,000	188	362	41.8	190	41.6	11.5	70.9	8.41	95.6	16.3	57.1	8.83	67.0	11.6
3H-2, 130–150	17.4	1070	1,090	283	390	47.0	212	45.9	12.7	66.1	9.50	107	18.1	62.6	9.77	71.4	12.4
3H-4, 130–150	20.4	563	183	84	124	13.1	61	13.0	3.96	31.9	3.53	44.5	8.1	31.3	5.23	42.2	7.62
4H-3, 130–150	28.4	1160	1,110	257	346	38.9	178	39.3	11.4	64.4	9.34	109	19.0	68.7	11.3	88.0	16.2
4H-5, 130–150	31.3	1230	1,600	105	115	18.4	97	23.3	7.22	46.1	7.06	91.3	17.3	63.6	10.3	78.4	14.2
5H-2 mud, 0–40	34.6	262	809	25	19.3	2.4	13	3.4	1.09	18.0	1.15	15.3	3.3	14.0	2.53	22.4	4.43
5H-2 sand, 0–40	34.6	771	116	108	197	22.8	104	23.5	8.73	34.2	5.19	66.4	12.0	46.2	7.85	61.6	11.6
6H-3, 110–150	47.7	697	575	1430	120	15.5	75	16.9	5.14	28.6	4.64	61.3	11.8	44.9	7.61	61.6	11.4
6H-5, 110–150	50.4	926	1,050	1170	120	16.7	83	19.3	6.38	48.0	5.67	71.9	13.6	52.6	9.01	72.4	13.9
7H-3, 110–150	56.9	820	884	467	121	16.9	83	20.0	6.36	70.7	5.30	66.3	12.5	47.9	8.05	65.5	11.9
8H-1, 110–150	63.2	743	513	1610	133	19.8	88	19.0	5.55	36.6	4.72	59.6	10.9	41.4	6.75	55.9	9.69
9H-5, 110–150	78.7	679	1,301	328	111	14.9	70	16.5	4.87	34.5	4.10	53.6	10.1	41.0	7.36	63.4	12.4
10H-1, 110–150	82.2	865	1,970	222	125	16.7	82	19.5	5.71	43.0	5.39	68.8	13.5	54.2	9.34	74.6	14.8
11H-1, 110–150	91.7	724	1,710	344	155	20.0	93	20.7	6.07	38.6	5.37	66.6	12.3	46.5	7.87	63.2	12.6
13H-1, 110–150	110.7	744	135	215	173	19.0	87	18.0	7.80	41.4	4.62	59.8	11.6	46.6	8.41	68.6	14.9
15H-1, 110–150	179.2	198	163	117	194	22.7	97	19.3	4.24	21.0	2.72	26.8	3.9	12.0	1.69	10.6	1.84
15H-4, 110–150	183.7	47	438	231	33.1	3.0	12	2.0	0.56	3.4	0.43	3.9	0.7	2.3	0.36	2.4	0.52
16H-2, 110–150	190.2	86	363	72	43.8	3.9	18	2.8	0.76	4.5	0.53	6.2	1.2	4.0	0.59	4.1	0.77
17H-2, 110–150	238.4	29	656	61	14.7	1.9	8	1.3	0.43	2.7	0.25	2.6	0.4	1.6	0.20	1.6	0.30
17H-5, 110–150	242.9	18	3,030	53	8.4	0.8	4	0.7	0.19	2.4	0.13	1.3	0.3	0.9	0.12	0.9	0.17
18H-2, 110–150	248.9	41	2,200	68	13.1	1.5	6	1.2	0.33	2.2	0.27	3.0	0.6	2.0	0.27	2.1	0.43
18H-4, 110–150	251.9	41	2,060	77	17.9	1.6	7	1.4	0.38	2.0	0.26	2.8	0.6	2.2	0.28	1.9	0.38
19H-1, 110–150	256.9	228	2,520	107	69.3	7.3	33	6.5	2.00	10.6	1.50	17.6	3.1	10.3	1.42	9.1	1.52
19H-2, 110–150	258.4	NA	NA	NA	NA	NA	NA	NA	NA	NA	NA	NA	NA	NA	NA	NA	NA
19H-3, 110–150	259.9	35	5,140	125	16.1	1.4	6	0.9	0.30	1.8	0.22	2.4	0.5	1.7	0.26	2.1	0.32
19H-4, 110–150	261.4	48	2,830	119	24.9	2.1	9	1.5	0.41	2.6	0.31	3.6	0.7	2.5	0.34	2.5	0.48
301-U1301D-																	
1H-1, 110–150	121.1	274	5,440	147	50.5	5.7	26	5.4	1.71	19.9	1.39	17.2	3.3	12.3	1.88	15.2	2.64
2H-1, 98–118	130.5	NA	NA	NA	NA	NA	NA	NA	NA	NA	NA	NA	NA	NA	NA	NA	NA
2H-2, 110–150	131.8	275	1,440	155	82.2	9.7	42	8.2	2.55	13.4	1.72	21.1	3.5	13.0	1.80	14.4	2.35
3H-2, 132–150	141.8	NA	NA	NA	NA	NA	NA	NA	NA	NA	NA	NA	NA	NA	NA	NA	NA
3H-3, 14–54	142.1	326	1,070	196	69.9	7.5	35	6.7	1.96	12.3	1.77	21.1	3.7	13.8	2.03	14.7	2.42
4H-2, 110–150	151.1	300	451	131	67.0	7.1	32	6.3	2.01	10.5	1.39	18.2	3.4	12.4	1.86	13.5	2.41
5H-1, 110–150	159.1	297	326	192	101	10.7	46	8.9	7.47	13.8	1.81	20.6	3.5	12.1	1.71	12.4	1.98
5H-5, 0–40	164.0	279	1,700	115	114	12.2	52	9.5	2.83	14.4	1.90	21.9	3.8	12.7	1.90	13.3	2.30
6H-2, 110–150	170.1	104	7,700	51	33.9	3.5	16	2.7	0.83	5.8	0.57	6.7	1.1	4.0	0.58	4.6	0.76
Error (±)		14	70	5	0.3	0.4	2	0.4	0.13	0.4	0.09	1.3	0.2	0.8	0.15	0.9	0.18
Detection limit		1.1	7	0.6	0.6	0.06	0.2	0.14	0.14	0.19	0.014	0.18	0.02	0.13	0.016	0.09	0.016
Bottom seawater		236	1,010	45	3.9	5.3	24	4.3	1.26	8.6	1.15	14.2	2.7	9.6	1.47	10.2	1.87

Table T2. Ge and Ge/Si composition of pore water, Holes 1024B and 1025B.

Core, section, interval (cm)	Depth (mbsf)	Ge (pmol/kg)	Ge/Si (µmol/mol)
168-1024B-			
1H-2, 140–150	2.95	537	1.2
1H-3, 140–150	4.45	686	1.4
1H-5, 140–150	7.33	1270	2.5
2H-2, 140–150	10.55	501	1.0
2H-5, 140–150	15.05	921	1.6
4H-5, 140–150	34.05	3280	5.8
9H-5, 140–150	81.55	2940	4.7
10H-5, 135–150	91.03	3360	5.8
11H-5, 135–150	100.53	1930	5.2
15X-5, 135–150	138.63	1740	2.0
17X-5, 135–150	157.83	2360	2.5
18X-2, 135–150	162.93	3530	4.9
18X-3, 135–150	164.43	2040	3.0
18X-4, 135–150	165.93	1760	2.4
18X-5, 135–150	167.43	631	1.2
168-1025B-			
1H-2, 140–150	2.95	542	1.2
1H-3, 140–150	4.45	795	1.7
2H-1, 140–150	6.45	1680	3.3
2H-2, 140–150	7.95	1140	2.2
2H-4, 140–150	10.95	1070	2.2
10X-1, 135–150	82.53	2120	5.3
10X-5, 135–150	88.53	1740	4.1

Notes: Data from Wheat et al. (2003, 2004). OSMO = OsmoSampler collection in sealed boreholes, CORK = direct sampling of the producing boreholes by submersible. Errors for the analysis are the same as those given in Table T1.

Table T3. Ge and Ge/Si composition of pore water from direct borehole sampling, Holes 1024C, 1027C, 1025B, and 1026B.

Core, sample, date	Depth (mbsf)	Ge (pmol/kg)	Ge/Si (µmol/mol)
168-OSMO1024C-			
60, 04-18-04	165.6	662	16
75, 03-05-03	165.6	688	16
112, 11-22-02	165.6	871	19
126, 10-20-02	165.6	790	17
168-OSMO1027C-			
27, 08-10-03	624	21,300	66
55, 07-05-03	624	16,200	51
106, 04-20-03	624	22,200	68
168-CORK1025B			
3472 Red, 1999	147.2	8,100	14
3472 Blue, 1999	147.2	8,290	14
3608 Red, 2000	147.2	9,560	17
168-CORK1026B			
3466 Red, 1999	295.2	22,300	31
3476 Red, 1999	295.2	20,100	27
3607 Blue, 2000	295.2	18,400	28
3607 Yellow, 2000	295.2	16,700	24

Notes: Data from Wheat et al. (2003, 2004). OSMO = OsmoSampler collection in sealed boreholes, CORK = direct sampling of the producing boreholes by submersible. Errors for the analysis are the same as those given in Table T1.

Table T4. Germanium and silica composition of pore waters in gravity core sediments from the southern EPR (EXCO) and Cocos Ridge (TicoFlux) flanks.

Cruise, core, location	Depth (mbsf)	Si (µmol/kg)	Ge (pmol/kg)	Ge/Si (µmol/mol)
TicoFlux-				
GC50; 9°5.045′N, 87°5.93′W				
	0.00	180	130	0.72
	0.13	222	268	1.21
	0.27	428	1332	3.11
	0.39	290	366	1.26
	0.59	367	746	2.04
	0.70	469	1280	2.73
	1.25	324	859	2.65
	1.33	224	369	1.65
GC40; 9°5.045′N, 87°5.93′W				
	0.00	180	130	0.72
	0.07	450	919	2.04
	0.12	435	906	2.08
	0.24	324	405	1.25
	0.45	257	419	1.63
	0.70	217	608	2.81
	0.91	403	695	1.72
	1.13	457	991	2.17
	1.44	272	475	1.75
	1.64	217	224	1.04
	2.03	418	1680	4.02
EXCO-				
GC15; 14°16.47′S, 112°19.44′W				
	0.00	180	127	0.71
	0.08	188	113	0.60
	0.22	192	80	0.42
	0.54	198	83	0.42
	0.86	197	77	0.39
	1.44	188	78	0.42
	2.42	174	70	0.40
	2.99	166	72	0.44
GC17; 14°16.88′S, 112°19.84′W				
	0.00	180	127	0.71
	0.04	202	105	0.52
	0.19	214	80	0.38
	0.51	211	58	0.28
	0.95	213	60	0.28
	1.49	209	81	0.39
	2.25	181	64	0.35
	2.79	183	88	0.48
GC19; 14°16.54′S, 112°19.44′W				
	0.00	180	127	0.71
	0.11	178	56	0.31
	0.27	176	46	0.26
	0.55	187	86	0.46
	1.01	187	57	0.31
	1.44	182	63	0.34
	2.12	177	108	0.61
	2.37	180	116	0.64

Notes: The labels give the core number and latitude-longitude coordinates for the samples. Errors for Ge and Ge/Si are given in Table T1.

Table T5. Chemical composition of the solid-phase sediments, Hole U1301C.

Core, section, interval (cm)	Depth (mbsf)	Al (mg/kg)	Ca (mg/kg)	Fe (mg/kg)	Mg (mg/kg)	Mn (mg/kg)	Si (mg/kg)	Ti (mg/kg)	Ge (mg/kg)	Ge/Si (µmol/mol)
301-U1301C-										
1H-2, 2–3	1.5	76,800	24,500	46,500	18,900	862	237,000	4,770	0.736	1.20
1H-3, 68–69	3.68	81,700	21,000	55,600	22,000	864	219,000	5,000	0.610	1.08
2H-3, 41–42	8.51	85,600	16,000	54,200	21,300	786	229,000	5,070	0.614	1.04
2H-3, 41–42	8.51	88,100	16,300	56,200	21,700	803	235,000	5,200	0.587	0.97
2H-6, 0–1	12.6	81,100	21,000	42,100	15,700	568	252,000	5,090	0.698	1.07
3H-3, 3–4	17.63	94,600	41,200	61,800	23,000	1,220	267,000	7,510	0.804	1.16
3H-5, 3–4	20.63	85,600	27,200	55,300	20,100	1,110	213,000	4,900	0.646	1.17
3H-7, 7–8	23.37	83,600	32,600	52,200	19,700	1,230	212,000	6,000	0.496	0.90
4H-4, 2–3	28.62	74,300	27,300	39,900	16,300	693	248,000	4,290	0.428	0.67
4H-6, 1–2	31.61	91,500	24,600	56,200	21,700	1,020	232,000	5,220	0.735	1.23
4H-7, 1–2	33.11	91,600	28,200	55,000	21,400	991	246,000	5,360	0.687	1.08
5H-1, 99–100	34.59	65,400	27,700	29,100	13,200	832	278,000	3,330	0.560	0.78
5H-1, 99–100	34.59	69,400	28,500	28,500	12,300	563	298,000	3,640	0.437	0.57
6H-4, 0–1	47.6	84,300	31,500	57,600	22,900	1,110	218,000	5,680	0.474	0.84
6H-5, 0–1	49.1	78,500	39,200	51,300	20,700	985	241,000	5,470	0.667	1.07
6H-6, 0–1	50.6	76,200	27,000	33,800	14,500	625	274,000	3,720	0.796	1.12
7H-3, 109–110	56.69	71,200	30,700	28,900	11,200	564	283,000	3,440	0.695	0.95
8H-1, 99–100	63.09	73,900	28,500	25,400	10,600	510	291,000	2,970	0.509	0.68
9H-6, 15–16	79.25	96,900	15,100	60,700	21,900	1,020	236,000	4,910	0.715	1.17
10H-1, 99–100	82.09	67,600	28,700	31,000	12,100	623	304,000	3,630	0.613	0.78
11H-2, 25–26	92.35	85,700	25,700	47,300	18,600	1,040	256,000	4,910	0.783	1.18
13H-1, 97–98	110.57	90,900	20,600	59,700	24,300	1,120	226,000	5,010	0.610	1.04
13H-3, 27–28	112.87	90,400	19,100	58,300	23,400	989	231,000	5,440	0.758	1.27
15H-2, 0–1	179.6	85,600	23,600	49,800	20,000	851	239,000	4,810	0.719	1.16
15H-5, 0–1	184.1	28,700	253,000	19,600	8,100	5,130	82,100	1,530	0.215	1.01
16H-3, 0–1	190.6	84,300	30,500	40,400	16,300	722	262,000	4,690	0.597	0.88
17H-3, 0–1	238.8	85,700	14,900	59,900	23,900	1,030	219,000	4,990	0.904	1.60
17H-6, 0–1	243.3	76,400	70,900	46,000	19,900	5,830	197,000	4,190	0.641	1.26
18H-3, 0–2	249.3	85,400	12,200	61,300	23,200	1,440	225,000	4,860	0.593	1.02
18H-5, 0–3	252.3	88,600	14,300	54,700	22,500	1,340	225,000	5,080	0.605	1.04
19H-2, 0–4	257.3	88,200	23,400	53,600	22,400	1,870	234,000	4,780	0.820	1.35
19H-3, 0–5	258.8	77,100	57,400	52,900	20,300	1,670	212,000	4,240	0.626	1.14
% error		3	3	3	3	3	3	3	3	6

Notes: Analyses were conducted at OSU by inductively coupled plasma–atomic emission spectroscopy for all elements except Ge, which was analyzed by ICP-MS. The method is described in McManus et al. (2006).